Energy Engineering

Tech Science Press

http://doi.org/10.32604/ee.2026.084035

ARTICLE

Performance Simulation Research on Vapor Compression Condensation Heat Compensation Constant Temperature and Humidity Air Conditioning System under Low Humidity Conditions

Lianglei Yin[1], Shuhong Li[1,*], Jun Wu[2], Jianbing Zhu[2], Jingjie An[2] and Wei Sheng[3]

[1]School of Energy and Environment, Southeast University, Nanjing, China
[2]Jiangsu Institute of Metrology, Nanjing, China
[3]Nanjing Bosen Technology, Nanjing, China
[*]Corresponding Author: Shuhong Li. Email: equart@seu.edu.cn

Received: 15 April 2026; Accepted: 17 June 2026; Published: 06 August 2026

ABSTRACT: To reduce the reheating energy consumption in traditional constant temperature and humidity air conditioning systems, a constant temperature and humidity air conditioning system with condensation heat compensation function is proposed. This system performs reheating treatment on the supply air by combining condensation heat recovery with electric heating, realizing decoupled control of temperature and humidity and ensuring control accuracy. A system model and corresponding experimental platform are established to verify the model's accuracy, and the experimental results show that the system has a temperature control accuracy of ±0.2°C and a relative humidity control accuracy of ±2%. Simulation results indicate that system performance is mainly affected by return air humidity and heat load. The evaporation temperature is mainly affected by return air humidity; when the return air humidity is lower than 25%, the evaporation temperature will reach the lower limit of 0°C, and the system will enter the extreme operating condition, while reducing the face velocity is conducive to increasing the evaporation temperature. The control parameters of heat recovery are mainly affected by return air humidity and heat-moisture load, which should be comprehensively considered during setting.

KEYWORDS: Constant temperature and humidity air conditioning system; condensing heat compensation; building energy efficiency; cooling dehumidification

1 Introduction

Driven by economic growth and technological progress, high-precision constant temperature and humidity air conditioning systems are now widely used as key facilities in scientific laboratories, data centers, manufacturing workshops, museums, and underground storage spaces [1–4].

Conventional constant temperature and humidity air conditioning systems mostly adopt an air processing strategy of "cooling prior to reheating", leading to considerable energy dissipation. Air conditioning systems incorporating rotary desiccant dehumidification or liquid desiccant dehumidification are confronted with disadvantages including bulky equipment configuration and high regeneration energy consumption [5–7]. In comparison, constant temperature and humidity air conditioning systems utilizing condensation heat recovery can achieve energy savings of 22.5%–38.2% [8], representing an effective approach to reducing reheat energy consumption.

A large body of academic investigations has been conducted on condensation heat recovery systems. Jia et al. [9] developed a hybrid dehumidification air-conditioning system, which achieved a 37.5% decrease in power consumption in experimental comparisons with conventional vapor compression air-conditioning systems. Yu et al. [10] recovered a portion of the condensation heat that was previously emitted into the soil and applied it to reheat the air in the air handling unit (AHU). Experimental data revealed that the indoor temperature and relative humidity were able to meet the standards outlined in the archive design code, while the operational cost was lowered by 48.4% in comparison to water-cooled units equipped with a boiler. Gong et al. [11] replaced the single air-cooled condensing module with an air conditioning/heat pump (AC/HP) system integrated with both air-cooled and water-cooled condensing modules. Their research results confirmed that the modified system displayed a higher coefficient of performance (COP) across all operating conditions.

Control precision is the key to constant temperature and humidity air conditioning systems. Qin et al. [12] established a PID control system combined with fuzzy control based on whale optimization algorithm. This strategy suppresses temperature overshoot in the passenger cabin by adjusting refrigerant circulation flow, and simultaneously improves the system COP. Wang et al. [13] proposed an intelligent adaptive fuzzy control method embedded with smoothing functions. In temperature regulation experiments, this method reduced the maximum control error by 29.4% and shortened the adjustment time by 35.7% compared with the conventional PID algorithm. Wu et al. [14] developed an improved segmented PID control strategy. By introducing segmented logic near the set value and appropriately weakening integral action, the system convergence speed was effectively enhanced. Xia et al. [15] put forward a model predictive control strategy to optimize temperature regulation and energy efficiency of direct expansion air conditioning systems. The results revealed that by coordinately controlling refrigerant circulation rate and air flow rate, the air supply temperature control accuracy could be improved to $\pm 0.5^{\circ}$C. Relevant studies have shown that the control precision of electric heating can reach $\pm 0.5^{\circ}$C, while that of condensation heat reheating can only reach $\pm 1^{\circ}$C [8,16,17].

Existing studies only focus on the effects of single condensation heat recovery on system performance or the influences of electric heating control strategies on control accuracy, lacking systematic exploration of hybrid operation modes that balance energy saving and control precision. Therefore, this paper proposes a constant temperature and humidity air-conditioning system with condensing heat recovery. The innovations of the proposed system are summarized as follows. The system adopts condensing heat to reheat supply air and employs electric heating to regulate return air temperature, which reduces energy consumption while ensuring high control accuracy. The direct condensing heat recovery method avoids intermediate heat transfer losses and reduces equipment size, making it suitable for practical engineering applications. Based on the proposed system, this paper investigates the effects of return air temperature and humidity, heat and moisture loads, and face velocity on system performance. The research results provide theoretical and practical references for designing high-precision and energy-saving air conditioning systems applicable to low-humidity environments.

2 System Introduction

The cooling and dehumidification air conditioning system with condensing heat recovery is shown in Fig. 1. The system mainly consists of a variable-frequency compressor, evaporator, condenser, heat recovery heat exchanger, energy regulating valve, and electronic expansion valve.

During the operation of the refrigeration system, high-temperature and high-pressure refrigerant gas discharged from the compressor enters the condenser and the heat recovery heat exchanger, where it is condensed into a medium-temperature subcooled liquid. After being throttled and depressurized by the electronic expansion valve, the refrigerant becomes a low-temperature and low-pressure vapor-liquid mixture and flows into the evaporator to undertake heat and mass transfer with indoor air. The vaporized refrigerant is then sucked back into the compressor to complete the cycle.

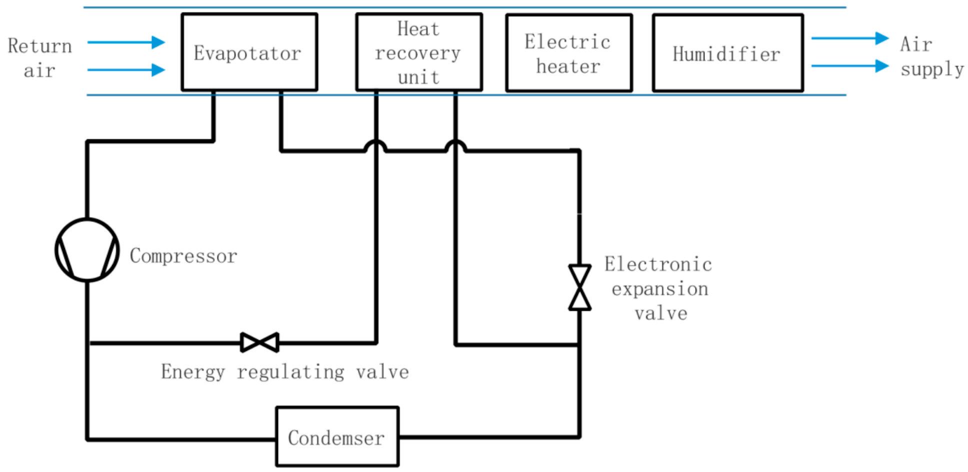

Figure 1: Schematic diagram of the condensing heat recovery air conditioning system.

The indoor return air first passes through the evaporator, where it is cooled and dehumidified on the evaporator surface. Subsequently, the air flows through the heat recovery heat exchanger, electric heater, and humidifier before being supplied into the room.

The adjustment for the continuous and stable operation of the system includes the following four basic points:

(1) Adjust the humidity of the air-conditioned area by regulating the compressor fre-quency;
(2) Adjust the temperature of the air-conditioned area by means of the electric heater;
(3) Adjust the superheat degree by regulating the opening degree of the electronic expansion valve;
(4) Adjust the outlet temperature of the heat recovery device by regulating the opening degree of the energy regulating valve.

2.1 Temperature Control Logic

The temperature control is shown in Fig. 2. Temperature control requires installing temperature sensor at the air-conditioned area.

The temperature sensor in the air-conditioned area is used to detect the temperature of the air-conditioned area and transmit the signal to the controller. According to the deviation between the real-time temperature value and the set value, the controller adjusts the temperature control component (i.e., the electric heater) to maintain the deviation within the control precision range.

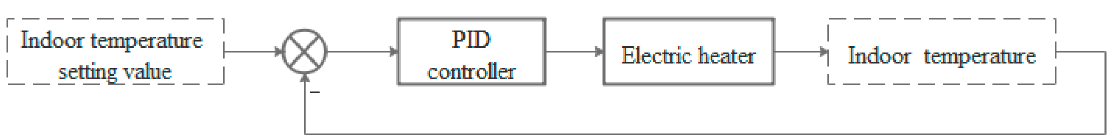

Figure 2: Temperature control schematic diagram.

2.2 Humidity Control Logic

Humidity control is shown in Fig. 3. Temperature and relative humidity sensors are installed in the air-conditioned area to detect the temperature and relative humidity of the air-conditioned area and transmit the signals to the controller. The controller calculates the dew point temperature according to the real-time temperature and relative humidity values of the air-conditioned area, and calculates the target dew point temperature according to the set temperature and relative humidity values. Then, the controller adjusts the humidity control devices (i.e., evaporator and humidifier) according to the deviation between the actual dew point temperature and the target dew point temperature, so as to maintain the deviation within the control precision range.

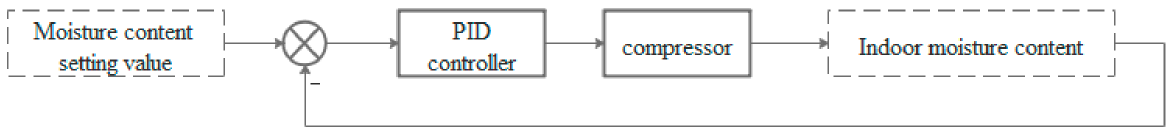

Figure 3: Humidity control schematic diagram.

In the humidification mode, the adjustment of the air-conditioned area relative humidity is realized through the humidifier.

On the one hand, the control logic needs to effectively adjust the relative humidity of the air-conditioned area; on the other hand, to ensure the normal operation of the air conditioning system and eliminate the frosting phenomenon, it is necessary to ensure that the surface temperature of the evaporator is higher than 0°C. The method of directly controlling the evaporation temperature and keeping it always above 0°C is adopted to prevent frosting. A pressure sensor is installed on the evaporator to detect the refrigerant pressure inside the evaporator, that is, the evaporation pressure, and transmit the detected signal to the controller. The controller calculates the real-time evaporation temperature inside the evaporator according to the evaporation pressure.

The control logic adjusts the evaporation temperature by changing the compressor frequency: when the evaporation temperature is lower than the critical value (0°C), the controller reduces the compressor frequency to reduce the refrigerant flow rate, thereby increasing the evaporation temperature; when the evaporation temperature is higher than the critical value, the controller increases the compressor frequency to increase the refrigerant flow rate, so that the evaporation temperature drops to the critical value and remains stable. When the indoor dew point temperature is too high and the dehumidification demand increases, the controller gradually increases the compressor frequency to enhance the dehumidification capacity, while strictly monitoring the evaporation temperature to prevent it from dropping below the critical value (0°C) due to excessive frequency increase, which may cause frosting on the evaporator surface.

2.3 Control Logic of Condensation Heat Recovery

The control of condensing heat recovery is shown in Fig. 4. When the temperature of the air-conditioned area is lower than the set value, the controller records the air temperature at the outlet of the heat recovery device at this time and gives an increment to the air temperature at the outlet of the heat recovery device. The controller controls the opening degree of the energy regulating valve to adjust the air temperature at the outlet of the heat recovery device, and reheats the supply air together with the electric heater. By adjusting the increment of the air temperature at the outlet of the heat recovery device, the ratio of electric heating to condensation heat recovery can be adjusted, so as to achieve the purpose of reducing the energy consumption of the system.

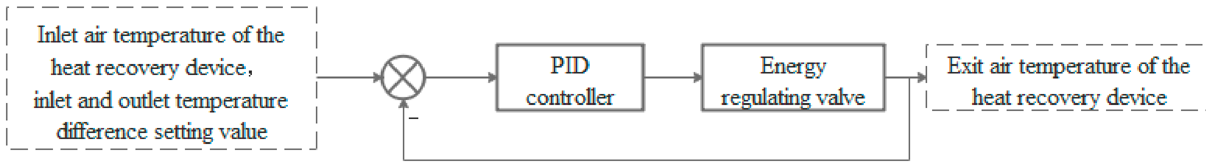

Figure 4: Condensing heat recovery control schematic diagram.

3 Model Establishment

3.1 Evaporator Model

The refrigerant inside the evaporator undergoes phase change, which is described using the multi-region moving boundary method.

In the superheated region, the refrigerant vapor experiences single-phase forced flow inside the evaporator tube, and its convective heat transfer coefficient is calculated using the Petukhov-Popov equation:

$$h_{eva.sh} = \frac{\lambda}{D_i}\frac{(f/8)Re \cdot Pr}{1.07 + 12.7(f/8)^{0.5}\left(Pr^{2/3} - 1\right)}, \tag{1}$$

$$f = (1.82lgRe - 1.64)^{-2}, \tag{2}$$

$h_{eva,sh}$: the convective heat transfer coefficient inside the tube in the superheated region, in W/(m^2·K);
f: the turbulent friction factor, applicable for Re = 10^4–5×10^6 and Pr = 0.5–2000.

For refrigerant boiling inside the evaporator, the local heat transfer coefficient of the refrigerant in the two-phase region is calculated using Schrock-Grossman equation [18]. The average heat transfer coefficient in the two-phase region is obtained by integrating the local heat transfer coefficient over the full range of vapor quality;

$$h_{eva,tp}(x) = 2.5X_{tp}^{-0.75} \cdot hl, \tag{3}$$

$$X_{\mathrm{tp}} = (\frac{1-x}{x})^{0.9} \cdot (\frac{\rho v}{\rho_l})^{0.5} \cdot (\frac{\mu_l}{\mu_v})^{0.1}, \tag{4}$$

X_{tp}: the Martinelli parameter;
x: Refrigerant dryness;
$h_{eva,tp}$: the convective heat transfer coefficient inside the tube in the two-phase region, in W/(m^2·K);
h_l: the liquid-phase convective heat transfer coefficient, calculated using Eqs. (12)–(14);
ρ_v: the vapor density, in kg/m^3;
ρ_l: the liquid density, in kg/m^3;
μ_v: the vapor dynamic viscosity, in Pa·s;
μ_l: the liquid dynamic viscosity, in Pa·s.

The evaporator adopts a sinusoidal corrugated fin heat exchanger. The air-side heat transfer coefficient under dry conditions is calculated using the correlation from Ref. [19], and the heat transfer factor is determined by Eq. (6).

The moisture coefficient $\xi = 1$ under dry conditions, while $\xi > 1$ under wet conditions. When condensate appears on the evaporator, the external surface heat transfer coefficient is considered to be ξ times that under dry conditions. Therefore, the heat transfer coefficient under wet conditions is calculated by Eq. (7).

$$\alpha_{\text{eva}} = jG_{\max} c_{pa} Pr^{-\frac{2}{3}}, \tag{5}$$

$$j = 0.196Re^{-0.318}(\frac{s}{D_o})^{0.309}(\frac{X_{\text{t}}}{P_{\text{d}}})^{0.163}, \tag{6}$$

$$\alpha_{eva,wet} = \xi \alpha_{eva}, \tag{7}$$

$$\xi = 1 + \frac{\gamma_0 + c_{pa} t_{a,ave} - c_{wat} t_{\text{w}}}{2c_{a,pm}} \cdot \frac{d_{a,ave} - d_{\text{w}}}{t_{a,ave} - t_{\text{w}}}, \tag{8}$$

α_{eva}: air-side heat transfer coefficient under dry conditions, in W/(m^2·K);
$G_{\max}$: mass flow rate of air at the minimum flow area of the fin, in kg/(m^2·s);
c_{pa}: specific heat of water vapor at constant pressure, in kJ/(kg·K);
Re: reynolds number based on the tube outside diameter;
D_o: tube outside diameter, in mm;
s: fin pitch, in mm;
X_{t}: fin projected length, in mm;
P_{d}: corrugation height, in mm;
$\alpha_{eva,wet}$: air-side heat transfer coefficient under wet conditions, in W/(m^2·K);
ξ: dehumidification factor;
γ_0: latent heat of vaporization of water, in kJ/kg;
c_{wat}: specific heat of water, in J/(kg·K);
$c_{a,pm}$: specific heat of moist air, in kJ/(kg·K);
$t_{a,ave}$: average temperature of the moist air entering and leaving the evaporator, in °C;
t_w: wall temperature, in °C;
$d_{a,ave}$: average moisture content of the moist air entering and leaving the evaporator, in g/kg dry air;
d_{w}: moisture content of saturated air corresponding to the wall temperature, in g/kg dry air.

In the evaporator model, the energy conservation equation is given by Eqs. (9)–(11).

$$Q_{eva,r} = m_r\left(H_{eva,r,i} - H_{eva,r,o}\right), \tag{9}$$

$$Q_{eva,r} = Q_{eva,a} = U_{eva} A_{eva} \Delta T_{eva}, \tag{10}$$

$$U_{eva} = \left[\frac{1}{\alpha_{eva,wet}} + \frac{\tau\delta}{\lambda} + \frac{\tau}{h_{eva}}\right]^{-1}, \tag{11}$$

$Q_{eva,r}$: heat transfer rates on the refrigerant side, in W;
$Q_{eva,a}$: heat transfer rates on air side, respectively, in W;
m_r: refrigerant mass flow rate, in kg/s;
$H_{eva,r,i}$: specific enthalpy of refrigerant at evaporator inlet, in J/kg;
$H_{eva,r,o}$: specific enthalpy of refrigerant at evaporator outlet, in J/kg;

U_{eva}: the overall heat transfer coefficient of the evaporator, in W/(m^2·K);
A_{eva}: the heat transfer area of the evaporator, in m^2;
ΔT_{eva}: the heat transfer temperature difference between the refrigerant and air sides of the evaporator;
τ: the fin coefficient;
δ: the tube wall thickness, in mm;
λ: the thermal conductivity of the tube wall, in W/(m·K);
h_{eva}: the convective heat transfer coefficient inside the evaporator tube, in W/(m^2·K).

3.2 Condenser and Heat Recovery Exchanger Model

For the refrigerant inside the condenser tubes, the correlation proposed by Dittus-Boelter [20] is adopted in the superheated and subcooled regions:

$$Nu_{con} = 0.023Re^{0.8}Pr^{n}, \tag{12}$$

$$h_{con,sh} = \frac{Nu_{con,sh} \cdot \lambda_{con,sh}}{D_i}, \tag{13}$$

$$h_{con,sc} = \frac{Nu_{con,sc} \cdot \lambda_{con,sc}}{D_i}, \tag{14}$$

When the fluid inside the tube is heated, n = 0.4; when cooled, n = 0.3.

d_i: the inner tube diameter, in mm;
$h_{con,sh}$: convective heat transfer coefficient inside the tube in the superheated region, in W/(m^2·K);
$h_{con,sc}$: convective heat transfer coefficient inside the tube in the subcooled region, in W/(m^2·K);
$Nu_{con,sh}$: Nusselt number in the superheated region;
$Nu_{con,sc}$: Nusselt number in the subcooled regions;
$\lambda_{con,sh}$: thermal conductivity of the refrigerant in the superheated region, in W/(m·K);
$\lambda_{con,sc}$: thermal conductivity of the refrigerant in the subcooled regions, in W/(m·K).

The heat transfer coefficient in the two-phase region $h_{c,tp}$ is given by Eq. (15) [21].

$$h_{con,tp} = h_{con,sc}\left[(1-x)^{0.8} + \frac{3.8x^{0.76}(1-x)^{0.04}}{{Pr_{con,tp}}^{0.38}}\right]. \tag{15}$$

The condenser adopts a sinusoidal corrugated fin heat exchanger, and its air-side heat transfer coefficient under dry conditions is calculated using Eqs. (5) and (6).

The heat recovery unit uses plain fins, and its air-side convective heat transfer coefficient can be calculated by Eq. (16) proposed by A.A. Гоголин.

$$\alpha_{reh} = C_1C_2(\frac{\lambda}{D_o})(\frac{L}{D_o})^{n}Re^{m}, \tag{16}$$

L: the fin length along the air flow direction, in m;
D_o: the equivalent diameter of the air flow channel cross-section, in m;
C_1: a parameter related to the air flow state;
C_2: a parameter related to the structural dimensions, whose calculation method is given by Eqs. (17)–(20).

$$C_1 = 1.36 - 0.0024Re, \tag{17}$$

$$C_2 = 0.518 - 2.315 \times 10^{-2}(\frac{L}{D_o}) + 4.25 \times 10^{-4}(\frac{L}{D_o})^2 - 3 \times 10^{-6}(\frac{L}{D_o})^3, \tag{18}$$

$$n = -0.28 + 8 \times 10^{-5} Re, \tag{19}$$

$$m = 0.45 + 0.0066 \frac{L}{D_o}. \tag{20}$$

In the condenser model, the energy conservation equation is given by Eqs. (21)–(23).

$$Q_{con,r} = m_r \left(H_{con,r,i} - H_{con,r,o} \right), \tag{21}$$

$$Q_{con,r} = Q_{con,a} = U_{con} A_{con} \Delta T_{con}, \tag{22}$$

$$U_{con} = \left[\frac{1}{\alpha_{con}} + \frac{\tau \delta}{\lambda} + \frac{\tau}{h_{con}} \right]^{-1}, \tag{23}$$

$Q_{con,r}$: heat transfer rate on the refrigerant side, in W;
$Q_{con,a}$: heat transfer rate on the air side, in W;
$H_{con,r,i}$: specific enthalpy of refrigerant at condenser inlet, in J/kg;
$H_{com,r,o}$: specific enthalpy of refrigerant at condenser outlet, in J/kg;
U_{con}: the overall heat transfer coefficient of the condenser, in W/(m^2·K);
A_{con}: the heat transfer area of the condenser, in m^2;
ΔT_{con}: the heat transfer temperature difference between the refrigerant and air sides of the condenser, in K;
h_{con}: the convective heat transfer coefficient inside the condenser tube, in W/(m^2·K).

The energy conservation equation for the heat recovery unit is the same as that for the condenser.

3.3 Compressor and Expansion Model

In the expansion valve model, it is assumed that the inlet enthalpy equals the outlet enthalpy:

$$H_{ev,i} = H_{ev,o}, \tag{24}$$

$H_{ev,i}$: specific enthalpy of refrigerant at the expansion valve inlet, in J/kg;
$H_{ev,o}$: specific enthalpy of refrigerant at the expansion valve outlet, in J/kg.

The variable-speed compressor is modeled using the lumped parameter method. The refrigerant mass flow rate m_r and compressor input power W_{co} are given as follows:

$$m_r = \eta_v \frac{V_h}{3600 v_s}, \tag{25}$$

$$V_h = \frac{V \cdot n}{60}, \tag{26}$$

$$n = \frac{60 f_z (1 - s)}{p}, \tag{27}$$

$$W_{co} = \frac{m_r (H_{co,o} - H_{co,i})}{\eta_{co}}, \tag{28}$$

$$H_{co,o} = H_{co,i} + \frac{H_{co,o,s} - H_{co,i}}{\eta_s}, \tag{29}$$

η_v: volumetric efficiency;
η_s: indicated efficiency;
η_{co}: compressor total efficiency;
V_h: theoretical volumetric displacement;
v_s: specific volume at suction, in m^3/kg;
V: compressor cylinder volume;
n: compressor speed;
f_z: compressor frequency;
s: slip ratio;
p: number of motor pole pairs;
$H_{co,o,s}$: enthalpy of refrigerant at isentropic state with inlet condition under condensing pressure, in J/kg;
$H_{co,i}$: specific enthalpy of refrigerant at compressor inlet, in J/kg;
$H_{co,o}$: specific enthalpy of refrigerant at compressor outlet, in J/kg;

3.4 Fan Model

Reference formula for electric power consumption of condensing fan [22].

$$W_{fan} = \frac{Fq_v}{1000\eta_{fan}\eta_m\eta_{me}}, \tag{30}$$

$$F = \Delta p + \frac{1}{2}\rho u^2, \tag{31}$$

$$\Delta p = f \cdot \frac{N{G_{\max}}^2}{2\rho}, \tag{32}$$

$$f = 4.19\mathrm{Re}^{-0.3979}\left(\frac{s}{D_o}\right)^{0.8925}\left(\frac{X_f}{P_d}\right)^{0.0808}, \tag{33}$$

W_{fan}: Fan electric power consumption, in kW;
F: wind pressure, in Pa;
q_v: air volume flow rate, in m^3/s;
η_{fan}: fan efficiency;
η_m: mechanical efficiency;
η_{me}: Motor efficiency;
Δp: ventilation resistance of finned tube bundle, in Pa;
ρ: air density, in kg/m^3;
u: air flow velocity, in m/s;
N: number of tube rows in the flow direction.

The calculation of the indoor evaporator fan refers to Formula (34), and the rest are the same as those for the condensing fan.

$$F = \Delta p + \Delta p_1 + \Delta p_2 + \Delta p_3, \tag{34}$$

Δp_1: filter resistance;
Δp_2: outlet grille resistance;
Δp_3: external static pressure.

3.5 Model Coupling and Performance Calculation

Based on the aforementioned model, a system simulation program was developed, and its calculation process is shown in the Fig. 5. The system model is mainly composed of five sub-models: compressor, condenser, heat recovery unit, expansion valve, and evaporator. The next step of calculation is carried out only after each sub-model achieves iterative convergence. R410A is selected as the working fluid in accordance with the actual system, and its thermophysical properties are obtained by calling the REFPROP 7.0 program.

The coupling model is adopted to calculate the operating parameters of the system, including the effects of return air temperature, return air humidity, heat load, moisture load and face velocity on system performance. The total system energy consumption P and system COP are taken as the performance indicators, whose definitions are presented in Eqs. (35) and (36).

$$P = W_{co} + W_{df} + W_{eh}, \tag{35}$$

$$\mathrm{COP} = \frac{Q_{sum}}{P}, \tag{36}$$

W_{co}: Compressor power consumption;
W_{df}: Fan power consumption;
W_{eh}: Electric heater power consumption;
Q_{sum}: Total indoor heat and moisture load.

To intuitively analyze the influence of condensing heat recovery capacity on the system, the heat recovery ratio ε is defined and calculated as shown in Eq. (37). When $\Delta t_{a,reh} = 0$, $\varepsilon = 0$; when $\Delta t_{a,reh} = \Delta t_{a,reh,max}$, $\varepsilon = 1$. In the simulation, the recovered heat is calculated from a specified heat recovery ratio. Afterwards, the supply air flow rate is adopted to compute the air temperature difference between the inlet and outlet of the heat recovery device. Taking this temperature difference as the actual operating temperature difference, the power consumption and COP corresponding to the given heat recovery ratio can be further obtained.

$$\varepsilon = \frac{Q_{reh}}{Q_{reh} + Q_{ele}}. \tag{37}$$

3.6 Model Validation

The evaporator, condenser and compressor are the main components of the system. To verify the accuracy of the models for the compressor, evaporator and condenser, an experimental platform of a constant temperature and humidity air conditioning system with condensing heat recovery was built in this study.

The experimental system consists of a 5 HP nominal capacity Copeland variable-speed compressor, an electric heater with a rated power of 9 kW, a humidifier with a rated power of 7.5 kW, and one evaporator, one condenser and one heat recovery unit, respectively. The refrigerant used is R410A.

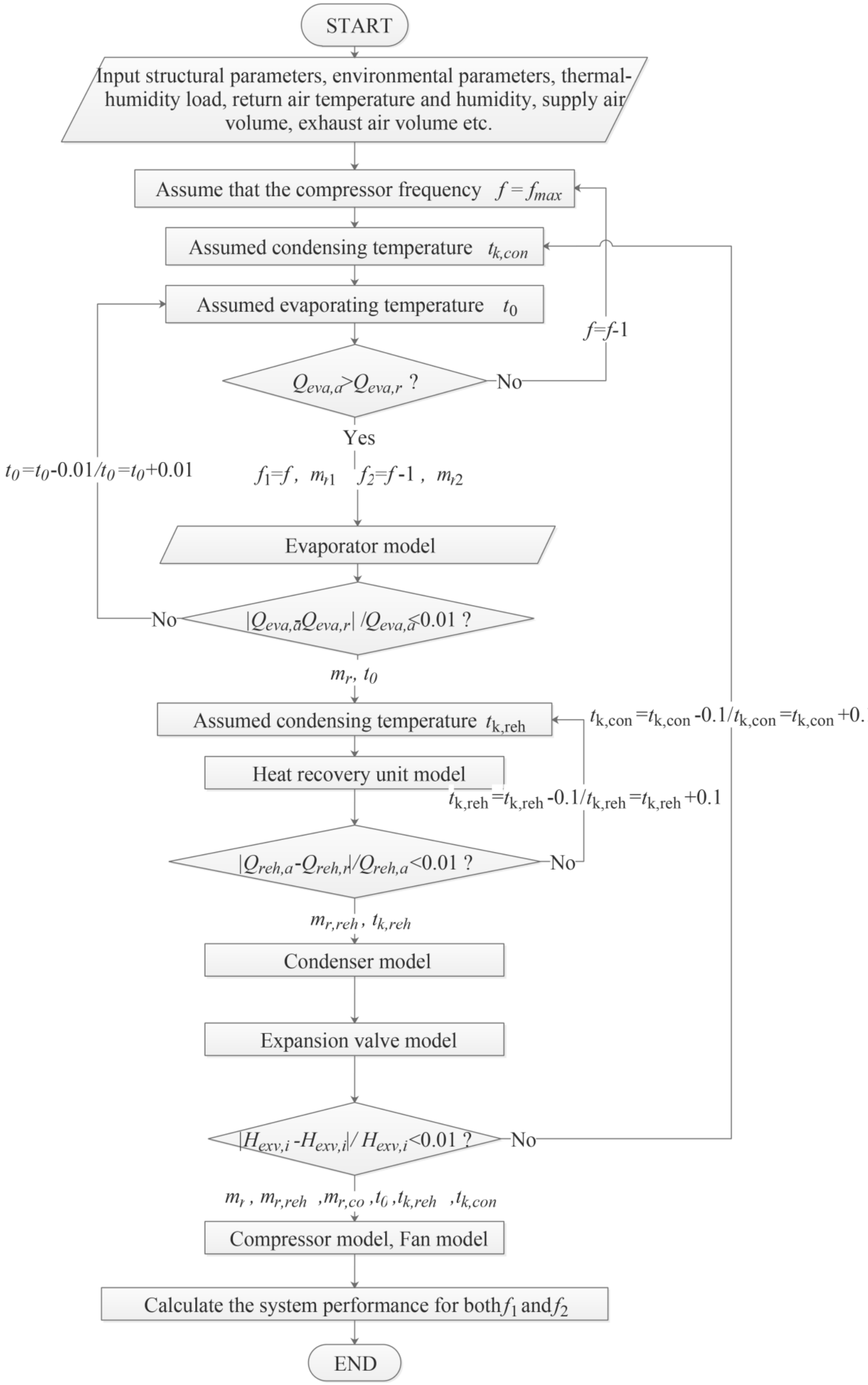

Figure 5: System algorithm flowchart.

The performance parameters of the compressor are listed in Table 1, and the structural parameters of the evaporator, condenser and heat recovery unit are presented in Table 2.

Table 1: Compressor parameter table.

Displacement	38.3 cc/Rev
Frequency Range	15–120 Hz
Rotational Speed Range	900–7200 RPM
Volumetric Efficiency	$\eta_v = -1.12 \times 10^{-4} {f_z}^2 + 0.0142 f_z + 0.645$
Isentropic Efficiency	$\eta_s = -9.8 \times 10^{-5} {f_z}^2 + 0.012 f_z + 0.59$
Electrical Efficiency	$\eta_m = -1.82 \times 10^{-6} {f_z}^2 + 0.00216 f_z + 0.815,\ 15 < f_z < 75\text{Hz}$ $\eta_m = -1.2 \times 10^{-6} {f_z}^2 + 0.00048 f_z + 0.925,\ 75 < f_z < 120\text{Hz}$

Table 2: Heat exchanger parameters.

	Evaporator	**Condenser**	**Heat Recovery Exchanger**
Tube row number	4	3	2
Single tube length/mm	600	1150	600
Inner diameter of copper tube/mm	9.52	9.52	9.52
Copper tube thickness/mm	0.45	0.45	0.45
Hole pitch/mm	25.4	25.4	25.4
Row pitch/mm	22	22	22
Fin thickness/mm	0.115	0.115	0.115
Fin spacing/mm	2	1.8	1.8
Corrugation height/mm	1.5	1.5	/
Corrugated projection length/mm	5.56	5.56	/

The humidity control of the air-conditioned zone is realized by transmitting temperature and humidity signals from a temperature and humidity sensor to a humidity controller. Under dehumidification mode, the controller regulates the speed of the variable-speed compressor according to the deviation between the current dew point temperature and the target dew point temperature. Under humidification mode, the controller maintains the indoor humidity at a constant value by means of the electric humidifier. The temperature of the air-conditioned zone is controlled by the electric heater.

The measuring point layout of the experimental system is shown in the Fig. 6. In the Fig. 6, P denotes pressure measuring points, T denotes temperature measuring points, RH denotes relative humidity measuring points, v denotes velocity measuring points, and q_m denotes mass flow measuring points.

On the refrigerant side, temperature measuring points include those at the inlet and outlet of the compressor, the outlet of the evaporator, the outlet of the heat recovery unit, and the inlet of the electronic expansion valve. Pressure measuring points include those at the inlet of the evaporator and the outlet of the condenser. Flow measuring points include those at the inlet of the heat recovery unit and the measuring point for compressor speed.

On the air side, measuring points are arranged for return air temperature and humidity, temperature and humidity at the evaporator outlet, and temperature and humidity at the heat recovery outlet. The supply air volume is measured indirectly by an anemometer.

The compressor power was measured by obtaining the corresponding voltage and current using a clamp multimeter.

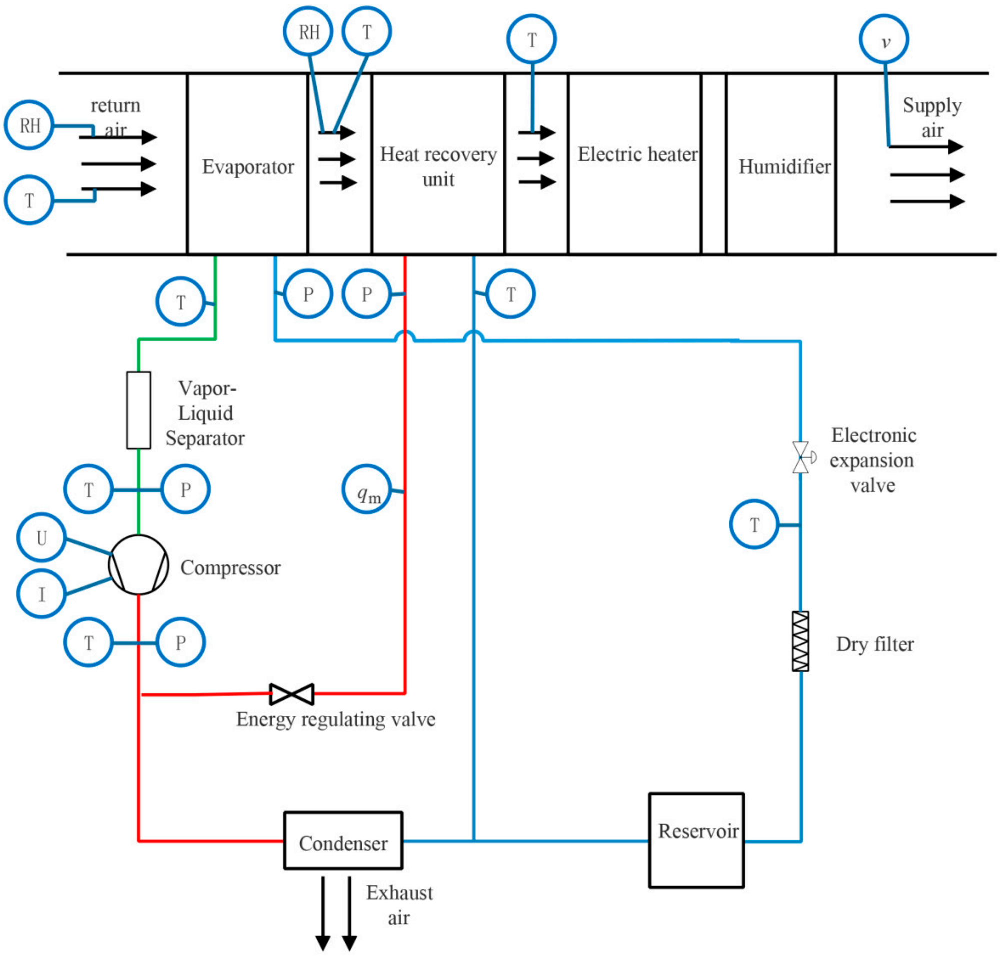

Figure 6: Experimental system measuring point layout.

The measuring instruments used in the experiment are listed in the Table 3.

Table 3: Measuring equipment information.

Name	Model	Error/Accuracy Class
Temperature and Humidity Sensor	EE210	±0.2°C, ±1.3%
Type-T Thermocouple	Type T	±0.5°C
Pressure Sensor	YCQB02L12	0.8% FS
Mass Flow Meter	PROMASS 83	±0.10%
Multimeter	KEW2200	±6 dgt
Anemometer	AS856S	±2.5%

In this work, the uncertainty of direct objects (such as temperature, pressure) can be represented by the following correlation:

$$u(x) \approx \sqrt{S_x^2 + \Delta_x^2}, \tag{38}$$

$u(x)$: the total uncertainty of measured value x;
S_x: the standard deviation of x;
Δ_x: the instrumental error.

The compressor power and air volume are obtained through indirect measurement, and the uncertainty of the measurement results refers to the following formula.

$$u(y) \approx \sqrt{\left(\frac{\partial y}{\partial x_1}\right)^2 u^2(x_1) + \left(\frac{\partial y}{\partial x_2}\right)^2 u^2(x_2) + \ldots + \left(\frac{\partial y}{\partial x_n}\right)^2 u^2(x_n)}. \tag{39}$$

Based on the cooling and dehumidifying air-conditioning system with condensation heat recovery, an experimental study was carried out with the return air temperature in the range of 22–28°C and the relative humidity in the range of 40%–75%. The experimental test results show that the temperature control precision of the system is ±0.2°C and the humidity control precision is ±2%.

First, the two sub-models of the evaporator and condenser were verified separately. The initial indoor ambient temperature of the experiment was 33°C, the relative humidity was 70%, the supply air volume was 5000 m^3/h, and the set target temperature and relative humidity were 26°C and 40%, respectively. During the 60 min of continuous operation of the unit, the evaporation temperature, condensation temperature, and air temperature at the evaporator outlet were verified. The verification results are shown in the Fig. 7. It can be seen from the figure that the experimental values are in good agreement with the simulated values and their changes are basically consistent. After calculation, the maximum error of the evaporation temperature is 1.48°C, the maximum error of the condensation temperature is 0.56°C, and the maximum error of the air temperature at the evaporator outlet is 1.33°C.

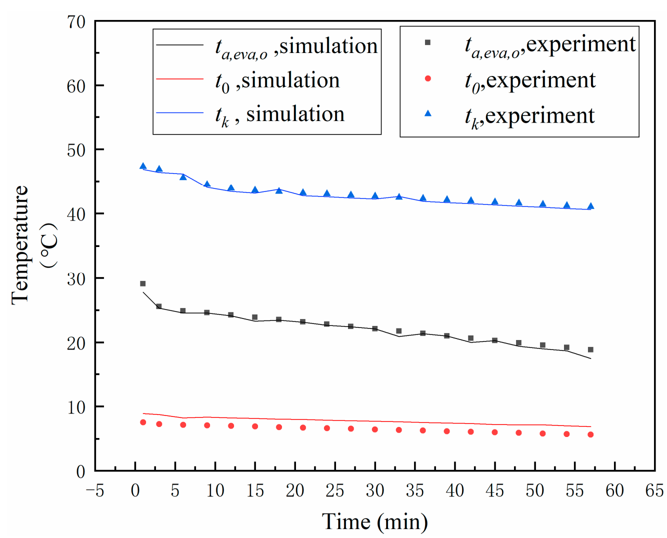

Figure 7: Model validation.

In addition, twelve sets of continuously stable operating conditions were selected under return air humidity ranging from 30% to 45% to verify the accuracy of the model under low humidity conditions. Each group of operating conditions was continuously and stably operated for no less than 5 min. The condensation temperature fluctuated within ±2°C and evaporation temperature fluctuated within ±1°C, the supply air temperature fluctuated within ±0.5°C, and the return air temperature fluctuated within ±0.2°C. The measured data were averaged to obtain the experimental operating condition range, which is shown in Table 4.

The experimentally measured parameters were substituted into the system model to verify the accuracy of the coupled model under 12 operating conditions. The evaporation temperature t_0, condensation temperature t_k, compressor power P_{co}, dehumidification capacity D, supply air temperature $t_{a,o}$, supply air relative humidity φ, heat recovery capacity Q_{reh} and total system power consumption P_{sum} were verified, respectively. The verification results are shown in Fig. 8. The results indicate that under the 12 operating conditions, the errors between the simulated and experimental values of evaporation temperature and condensation temperature are within ±10%, the error of compressor power is within ±15%, the error of dehumidification capacity is within ±12%, the error of supply air temperature is within ±8%, and the error of supply air humidity is within ±5%, the error of heat recovery capacity is within ±10%, and the total system power consumption error is within ±15%.

Table 4: Test conditions.

Supply Air Volume (m^3/h)	Return Air Temperature (°C)	Return Air Relative Humidity	Outdoor Temperature (°C)	Outdoor Relative Humidity	$\Delta t_{a,reh}$ (°C)
2800	25.0	41%	33.0	63%	2
2800	24.0	42%	36.3	70%	2
3500	25.7	45%	33.1	68%	2
3500	26.2	42%	33.6	70%	2
3500	25.0	42%	29.2	66%	2
2800	24.5	38%	28.5	65%	2
2800	23.0	45%	27.0	62%	2
1500	25.0	32%	29.0	62%	2
1500	24.0	33%	31.0	65%	2
1500	28.0	34%	28.6	60%	2
1500	26.5	30%	28.5	54%	2
1500	27.0	29%	30.1	51.%	2

In summary, the calculated results of the vapor-compression condensing heat recovery cooling and dehumidifying system model adopted in this study are all within a reasonable range, and the model can be used for further simulation research.

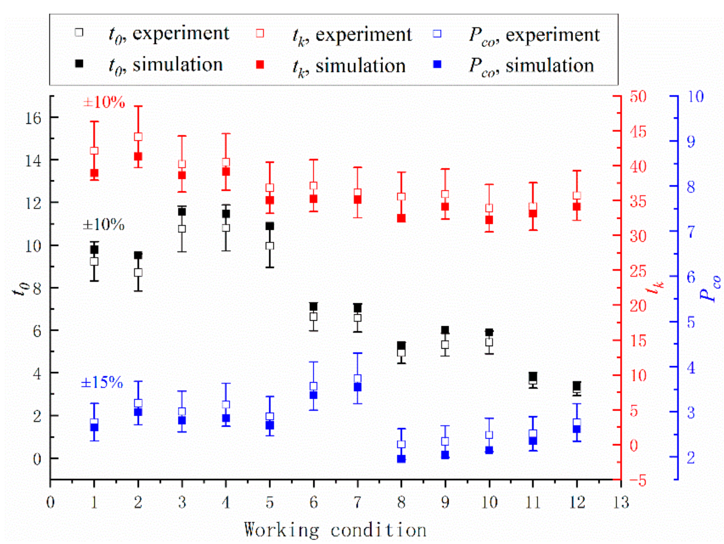

(a)

Figure 8: *Cont.*

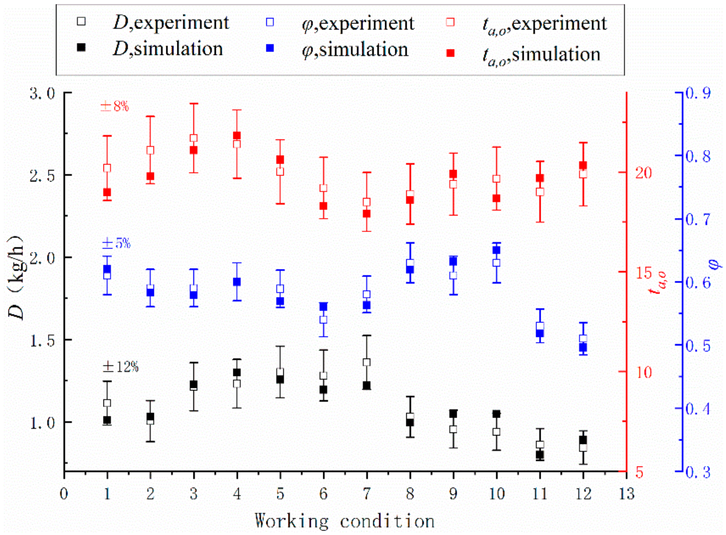

(**b**)

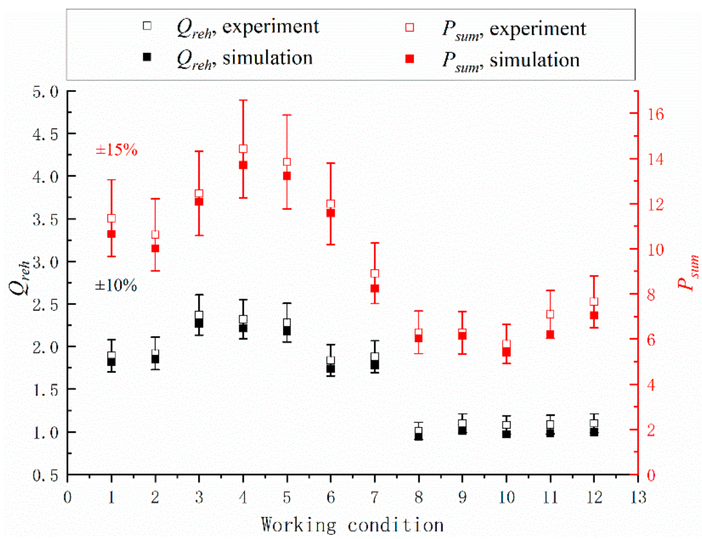

(**c**)

Figure 8: Model validation. (**a**) Verification of evaporation temperature, condensation temperature and compressor power (**b**) Verification of dehumidification capacity, supply air temperature and supply air humidity (**c**) Verification diagram of heat recovery capacity and total system power consumption.

4 Results and Discussion

Based on the above model, this paper studies the effects of return air temperature, return air humidity, heat load, moisture load, and face velocity on the system COP and energy consumption, and analyzes the impact of condensation heat recovery ratio on system energy efficiency. Meanwhile, to ensure the continuous and stable operation of the system, the effects of different operating conditions on evaporation temperature are analyzed. The set value of the air temperature difference $\Delta t_{a,reh}$ between the inlet and outlet of the heat recovery device is a key parameter to reduce reheating energy consumption and improve system performance. However, an excessively high set value of $\Delta t_{a,reh}$ may lead to the system being unable to provide sufficient cooling capacity. Therefore, this paper studies the effects of operating parameters on $\Delta t_{a,reh,max}$, providing guidance for the set value of $\Delta t_{a,reh}$.

4.1 Effects of Return Air Temperature on System Performance

The heat load was set at 10 kW, the moisture load at 1.5 kg/h, and the indoor return air humidity as well as ambient temperature and humidity were kept constant. The effect of return air temperature on system performance was investigated. It can be seen from the Fig. 9a that return air temperature has a relatively small influence on system energy consumption and COP. With the increase of return air temperature, the heat transfer temperature difference on the evaporator side increases, which is beneficial to heat transfer. Therefore, the system energy consumption decreases and the COP increases accordingly. Within the studied 7 operating conditions, when the heat recovery ratio ε = 0.9, compared with the case when the heat recovery ratio is 0, the system energy consumption is significantly reduced and the system COP is significantly improved, with an average energy consumption reduction of 62% and an average COP increase of 169.3%. This performance promotion is significantly superior to that of traditional electric reheating constant temperature and humidity systems reported in previous studies, which usually only achieve a maximum energy-saving rate of less than 40% under similar load conditions. The prominent performance advantage is mainly attributed to the direct condensing heat recovery structure adopted in this system, which eliminates intermediate heat transfer loss compared with the indirect heat recovery schemes in existing literature.

As shown in Fig. 9b, the air temperature difference between the inlet and outlet of the heat recovery device hardly changes with the change of return air temperature, while the evaporation temperature increases with the increase of return air temperature. The underlying mechanism is that a higher return air temperature can widen the heat transfer temperature difference while lowering the dew-point temperature of return air, which consequently raises the evaporating temperature.

However, such favorable performance cannot be generalized to all operating conditions. First, the positive correlation between return air temperature and system COP is only applicable to the medium return air temperature range adopted in this study. Second, compared with conventional systems, the energy-saving advantage of the proposed system is weakened under ultra-low indoor load conditions. In addition, restricted by the maximum heat release capacity of the heat recovery unit, the heat recovery ratio cannot be infinitely maintained at 0.9 under full working conditions, which is a key practical limitation of the system in engineering applications.

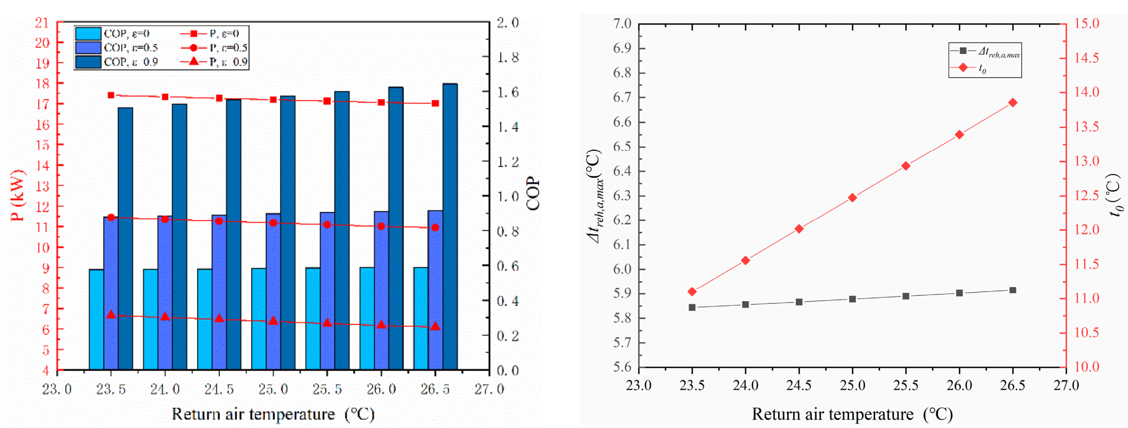

(**a**) (**b**)

Figure 9: Effect of return air temperature on system performance. (**a**) Effect of return air temperature on system COP and P; (**b**) Effect of return air temperature on t_0 and $\Delta t_{a,reh,max}$.

4.2 Effects of Return Air Humidity on System Performance

The heat load was set at 5 kW, the moisture load at 0.8 kg/h, and the indoor return air temperature as well as ambient temperature and humidity were kept constant. The operating performance of the system under low humidity conditions was studied. As shown in Fig. 10a, as the return air humidity increases from 15% to 45%, the average system energy consumption decreases by 75.4%, and the system COP is significantly improved.

As shown in Fig. 10b, when the return air humidity is less than 20%, the evaporation temperature is less than 0°C, making it difficult for the system to ensure continuous and stable operation. Therefore, for the air conditioning system studied in this paper, when the moisture load is 0.8 kg/h, continuous and stable operation can be guaranteed when the return air humidity is 25%. The return air humidity has an inverse relationship with the air temperature at the inlet and outlet of the heat recovery device, which is because the increase in humidity will reduce the reheating capacity. Physically, higher air moisture content reduces required reheat load, lowering the needed temperature lift across the heat recovery unit. Such negative correlation does not hold under overloaded indoor dehumidification demands, where insufficient recovered heat will reverse this changing trend and weaken system efficiency.

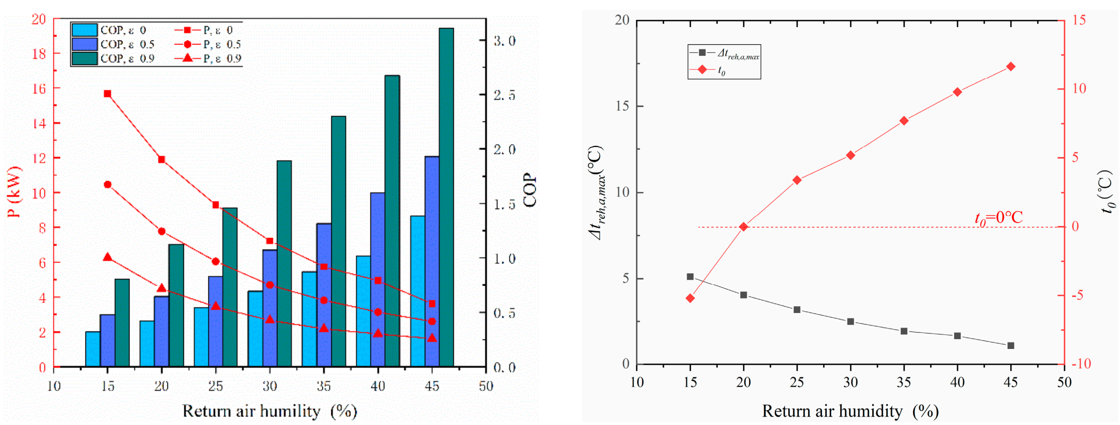

(**a**) (**b**)

Figure 10: Effect of return air humidity on system performance. (**a**) Effect of return air humidity on system COP and P; (**b**) Effect of return air humidity on t_0 and $\Delta t_{a,reh,max}$.

4.3 Effects of Heat Load on System Performance

The moisture load was set at 2 kg/h, and the indoor return air temperature and humidity as well as ambient temperature and humidity were kept constant. The influence of changes in heat load on system performance was investigated. As shown in Fig. 11a, the system energy consumption decreases with the increase of heat load, and the system COP increases with the increase of heat load. As the heat load increases from 8 kW to 14 kW, the average system energy consumption decreases by 53.2%, and the average system COP increases by 170.3%. With the increase of heat load, the system COP continued to rise under the three heat recovery ratios. When the heat recovery ratios were 0 and 0.5, the system power consumption decreased with the increase of heat load; when the heat recovery ratio was 0.9, the system power consumption increased slowly with the increase of heat load. This is because the increase of heat load reduces the reheat load, decreases the system heat recovery capacity, increases the condensing temperature, and thus increases the system power consumption. Compared with conventional non-reheat systems in published studies that only gain limited efficiency improvement under variable heat load, the direct condensation heat reuse delivers obvious energy benefits: relative to the baseline case ε = 0, ε = 0.5 yields an average 32.4% power cut, whereas ε = 0.9 achieves a 60.4% average power reduction.

As shown in Fig. 11b, the change of heat load has almost no effect on the evaporation temperature, while the increase of heat load has a significant impact on $\Delta t_{a,reh,max}$. This physical constraint highlights that indoor heat load must be prioritized during the design of target reheat temperature difference $\Delta t_{a,reh}$. A larger $\Delta t_{a,reh}$ will raise the heat load on one side and increase compressor power consumption accordingly; on the other side, it cuts off the electric heater, leading to indoor air temperature exceeding the setpoint.

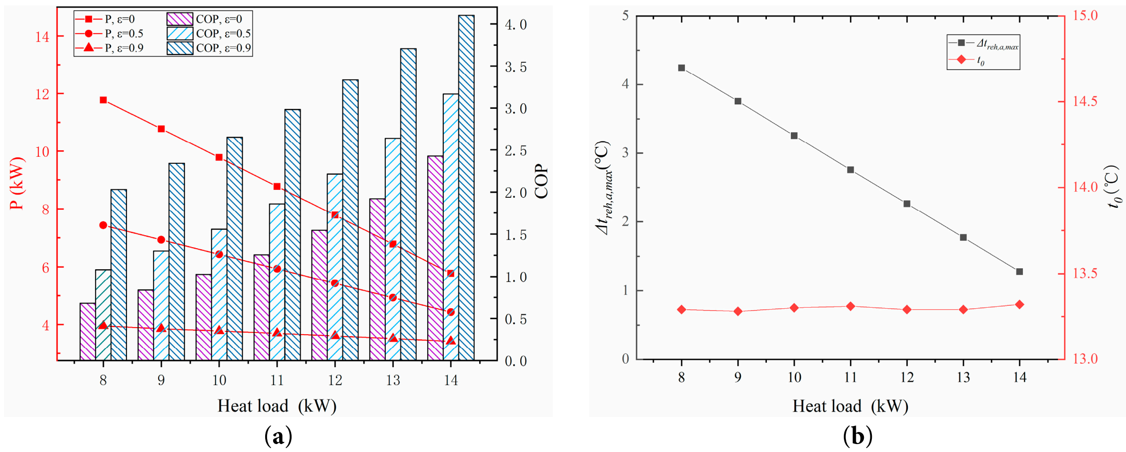

Figure 11: Effect of heat load on system performance. (**a**) Effect of heat load on system COP and P; (**b**) Effect of heat load on t_0 and $\Delta t_{a,reh,max}$.

4.4 Effects of Moisture Load on System Performance

The heat load was set at 10 kW, and the indoor return air temperature and humidity as well as ambient temperature and humidity were kept constant. As illustrated in Fig. 12a, system power consumption rises monotonically and COP declines gradually with growing moisture load across all three preset heat recovery ratios. From the thermodynamic perspective, elevated dehumidification demand lowers evaporating pressure, enlarges compressor compression ratio and power input, which inherently deteriorates overall COP. Compared with conventional electric-reheat constant temperature and humidity systems reported in existing literature, the proposed condensation heat recovery setup still retains obvious energy-saving superiority even under high moisture load, yet such advantage gradually shrinks as dehumidification requirement keeps growing. Notably, the above variation law is only valid within the tested load scope and cannot be generalized infinitely; when moisture load exceeds the upper limit of the heat recovery capacity, recovered condensation heat fails to cover full reheat demand, and the performance gap between the proposed system and traditional schemes will be further narrowed.

As shown in Fig. 12b, with the increase of moisture load, the evaporation temperature decrease continuously. In addition, $\Delta t_{a,reh,max}$ presents a positive correlation with moisture load. With fixed return air parameters, increased moisture load reduces evaporator outlet air temperature and raises the required reheat duty, which directly pushes up the maximum feasible reheat temperature difference. In practical engineering, excessive moisture load will cause $\Delta t_{a,reh,max}$ to exceed the upper limit available from condensation waste heat, forcing auxiliary electric heating to activate and offset part of the energy-saving benefit of the heat recovery system, which is an important practical constraint for engineering application.

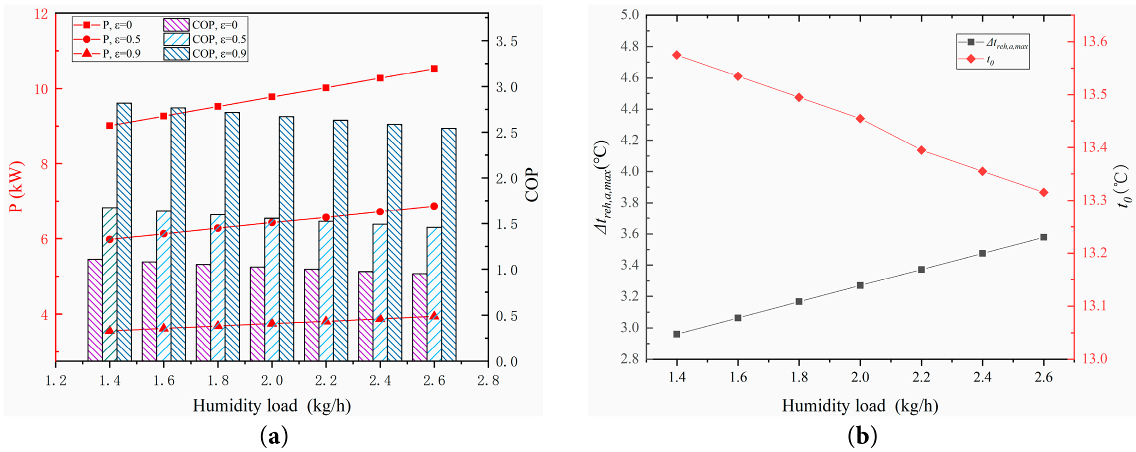

Figure 12: Effect of moisture load on system performance. (**a**) Effect of moisture load on system COP and P; (**b**) Effect of moisture load on t_0 and $\Delta t_{a,reh,max}$.

4.5 Effects of Face Velocity on System Performance

The heat and moisture loads, indoor return air temperature and humidity, as well as ambient temperature and humidity were kept constant. The influence of changes in face velocity on system performance was investigated. It can be seen from Fig. 13a that with the increase of face velocity, the system energy consumption continued to rise and the system COP continued to decrease. This is because when the moisture load is constant, the increase of face velocity reduces the dehumidification coefficient, increases the heat load on the evaporator side, and the increase of refrigerant flow rate leads to an increase in compressor energy consumption.

Nevertheless, such energy-saving superiority is not universally applicable. At excessively high face velocity, the growing evaporator cooling demand consumes most recovered condensation heat, sharply narrowing the performance gap between the proposed system and traditional non-recovery alternatives. In extreme cases, available waste heat is insufficient for full air reheating, triggering supplementary electric heating and further erasing the heat-recovery-derived energy benefit.

As can be seen from Fig. 13b, with the increase of face velocity, the evaporation temperature decreases continuously, while $\Delta t_{a,reh,max}$ increases continuously. This is because under the conditions of constant heat and moisture load as well as return air temperature and humidity, to meet the constant temperature and humidity requirements, the increase of air volume leads to an increase in the air-side heat transfer coefficient and the cooling load on the evaporator side. To meet the constant temperature and humidity requirements, the compressor increases its frequency, resulting in a decrease in evaporation temperature and an increase in refrigerant flow rate, which leads to a decline in system performance.

Different from findings in existing literature, reducing the coil face velocity improves system efficiency and elevates evaporation temperature under the operating conditions specified in this work. Nevertheless, excessively low face velocity substantially cuts the air-side heat transfer coefficient and impairs heat exchange. During practical operation, this will gradually pull down the evaporation temperature and raise overall system power consumption. From an engineering constraint perspective, an overlarge face velocity pushes $\Delta t_{a,reh,max}$ beyond the upper limit of recoverable condensation heat; this inherent physical restriction restricts the allowable maximum air velocity in practical unit design.

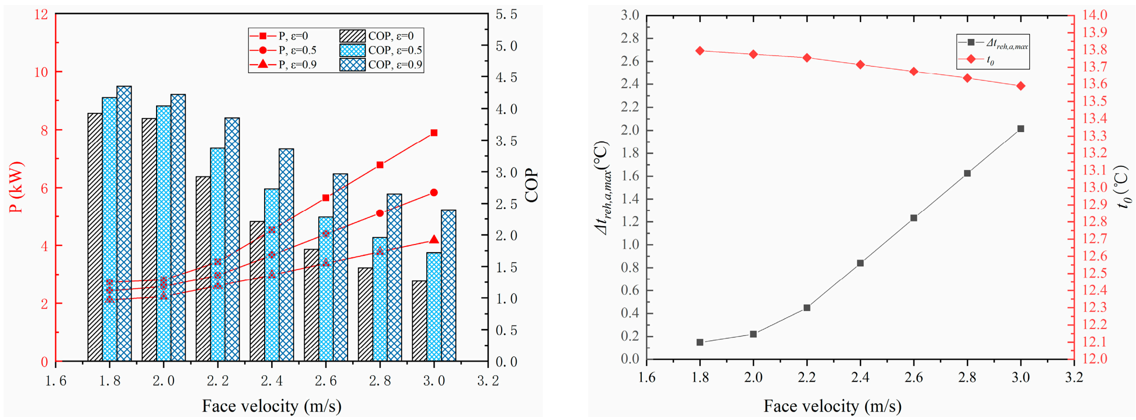

(**a**) (**b**)

Figure 13: Effect of face velocity on system performance. (**a**) Effect of face velocity on system COP and P; (**b**) Effect of face velocity on t_0 and $\Delta t_{a,reh,max}$.

5 Conclusions

This paper proposes a constant temperature and humidity air conditioning system with condensation heat recovery and establishes its system coupling model. An experimental platform for the proposed system is built to verify the accuracy of the established model. The effects of return air temperature (23.5–26.5°C), return air humidity (15%–45%), heat load (8–14 kW), moisture load (1.4–2.6 kg/h) and face velocity (1.8–3.0 m/s) on system performance are investigated via numerical simulation, and the main conclusions are drawn as follows:

(1) The proposed air conditioning system combining condensation heat recovery and electric heating can operate continuously and stably under summer conditions when the relative humidity is no less than 30%, with a temperature control accuracy of ±0.2°C and a relative humidity control accuracy of ±2%. Experimental results verify the reliability of the coupling model, which shows great consistency with measured data. The error of compressor power is within ±15%, and the errors of evaporation temperature and condensation temperature are within ±10%.

(2) Return air humidity and heat load exert remarkable influences on system performance. With the heat load at 5 kW, moisture load at 0.8 kg/h, and constant return-air temperature as well as outdoor ambient temperature and humidity, as the return air relative humidity rises from 15% to 45%, the average system energy consumption decreases by 75.4% and the system COP is greatly improved. With the moisture load at 2 kg/h, return air humidity is 45%, and constant return-air temperature as well as outdoor ambient temperature and humidity, as the heat load increases from 8 kW to 14 kW, the average system energy consumption drops by 53.2%, and the average system COP rises by 170.3%.

(3) Return air temperature and return air humidity have more prominent effects on evaporation temperature. With the heat load was set at 10 kW, the moisture load at 1.5 kg/h, and the indoor return air humidity as well as ambient temperature and humidity were kept constant, as the return air temperature increases from 23.5°C to 26.5°C, the evaporation temperature rises from 11.1°C to 13.9°C. When the return air relative humidity drops below 25%, the evaporation temperature falls below 0°C, posing a frosting risk to the heat exchanger.

(4) With indoor sensible heat load fixed at 10 kW, moisture load at 1.5 kg/h, return air temperature of 26°C and relative humidity of 45%, the evaporation temperature decreases gradually as the coil face

velocity rises from 1.8 m/s to 3 m/s. This variation trend differs from that of most conventional air conditioning systems, which can effectively avoid heat exchanger frosting.

(5) Return air humidity, heat load and moisture load significantly affect the maximum air temperature difference between the inlet and outlet of the heat recovery device, which decreases with the increase of return air humidity and heat load. Comprehensive consideration should be taken when setting the inlet-outlet temperature difference of the heat recovery device.

Acknowledgement: This study was funded by the National Natural Science Foundation of China (No. 52576009), National Natural Science Foundation of China (No. 52276002) and Jiangsu Market Supervisory Authority Scientific Research Project, China (KJ2025009).

Funding Statement: This study was funded by the National Natural Science Foundation of China (No. 52576009), National Natural Science Foundation of China (No. 52276002) and Jiangsu Market Supervisory Authority Scientific Research Project, China (KJ2025009).

Author Contributions: Conceptualization, Lianglei Yin; methodology, Lianglei Yin; software, Lianglei Yin; validation, Lianglei Yin; formal analysis, Lianglei Yin; resources, Jun Wu, Jianbing Zhu, Jingjie An, Wei Sheng, Shuhong Li; data curation, Lianglei Yin; writing—original draft preparation, Lianglei Yin; writing—review and editing, Lianglei Yin, Shuhong Li; visualization, Lianglei Yin; supervision, Shuhong Li; project administration, Shuhong Li; funding acquisition, Shuhong Li. All authors reviewed and approved the final version of the manuscript.

Availability of Data and Materials: The data supporting the findings of this study are available within the article.

Ethics Approval: Not applicable.

Conflicts of Interest: The authors declare no conflicts of interest. Two for-profit enterprises provided test sites and experimental equipment for this work. The relevant authors only participated in experimental supervision and received no financial benefits associated with this study, including research funding, patents, or commercial remuneration. No commercial products or proprietary technologies from the above enterprises were used in this research.

Nomenclature

A	The heat transfer area, m^2	*Greek symbols*	
c_{wat}	Specific heat of water, J/(kg·K)	ρ	Density, kg/m^3
$c_{a,pm}$	Specific heat of moist air, kJ/(kg·K)	μ	Dynamic viscosity, Pa·s
COP	Coefffcient of performance	α	Heat transfer coefficient, W/(m^2·K)
d	Air moisture, g/kg	ξ	Dehumidification factor
D	Pipe diameter, m	γ_0	Latent Heat of Vaporization, kJ/kg
f	The turbulent friction factor	τ	The fin coefficient
fz	Compressor frequency, Hz	δ	The tube wall thickness, mm
F	Wind pressure, Pa	λ	Thermal conductivity, W/(m·K)
G_{max}	Mass flow rate, kg/(m^2·s)	η	Efficiency
h	heat transfer coefficient, W/(m^2·K)	ε	Heat recovery ratio
H	Enthalpy, in J/kg	*Subscripts*	
j	Heat exchange factor	a	Air
m_r	Refrigerant mass flow rate, kg/s	ave	Average
n	Compressor speed, REV	co	Compressor
N	Number of tube rows	con	Condenser
Pr	Prandtl number	eva	Evapotator
p	Number of motor pole pairs	i	Inlet
q_v	Air volume flow rate, m^3/s	l	Liquid

Q	Heat transfer rates, W	m	Mechanical
Re	Reynolds number	me	Motor
s	Fin pitch, mm	o	Outlet
Sx	The standard deviation of x	r	Refrigerator
t	Temperature, °C	sc	Supercooling region
u	Velocity, m/s	sh	Overheated region
V	Compressor cylinder volume	tp	Two-phase region
W	Working, W	v	Vapor
		w	Wall

References

1. Yin J, Liu X, Guan B, Ma Z, Zhang T. Performance analysis and energy saving potential of air conditioning system in semiconductor cleanrooms. J Build Eng. 2021;37:102158. [CrossRef].
2. Wu J, Xu X, Liao X, Li Z, Zhang S, Huang Y. Intelligent diagnosis method of data center precision air conditioning fault based on knowledge graph. Electronics. 2023;12(3):498. [CrossRef].
3. Zhang XJ, Yu CY, Li S, Zheng YM, Xiao F. A museum storeroom air-conditioning system employing the temperature and humidity independent control device in the cooling coil. Appl Therm Eng. 2011;31(17–18):3653–7. [CrossRef].
4. Wang W, He MX, Liu CY, Zhang Y. The research of constant temperature and humidity air-conditioning system of underground cellar. Appl Mech Mater. 2014;672–674:1722–8. [CrossRef].
5. Qi R, Dong C, Zhang LZ. A review of liquid desiccant air dehumidification: From system to material manipulations. Energy Build. 2020;215:109897. [CrossRef].
6. Su W, Lu Z, She X, Zhou J, Wang F, Sun B, et al. Liquid desiccant regeneration for advanced air conditioning: A comprehensive review on desiccant materials, regenerators, systems and improvement technologies. Appl Energy. 2022;308:118394. [CrossRef].
7. Rafique MM, Rehman S, Alhems LM, Lashin A. Parametric analysis of a rotary type liquid desiccant air conditioning system. Energies. 2016;9(4):305. [CrossRef].
8. Jwo CS, Chen TY, Hsu CF, Chien LY, Tsai MY. Energy saving analysis on application of condensing heat recovery to constant temperature/humidity system. Appl Mech Mater. 2013;291–294:1805–11. [CrossRef].
9. Jia CX, Dai YJ, Wu JY, Wang RZ. Analysis on a hybrid desiccant air-conditioning system. Appl Therm Eng. 2006;26(17–18):2393–400. [CrossRef].
10. Yu X, Wang RZ, Zhai XQ. Year round experimental study on a constant temperature and humidity air-conditioning system driven by ground source heat pump. Energy. 2011;36(2):1309–18. [CrossRef].
11. Gong G, Zeng W, Wang L, Wu C. A new heat recovery technique for air-conditioning/heat-pump system. Appl Therm Eng. 2008;28(17–18):2360–70. [CrossRef].
12. Qin Z, Wang X, Zhang H, Liu F, Yin C, Han Z, et al. Research on heat pump air conditioner compressor speed control strategy based on whale algorithm. Case Stud Therm Eng. 2024;53:103939. [CrossRef].
13. Wang Y, Liu J, Yu J. Lyapunov-derived fuzzy temperature control for thermoelectric cooling system using dynamic updating law. Appl Therm Eng. 2025;258:124600. [CrossRef].
14. Wu G, Wu W. Research on algorithm based on improved PID controller. J Phys Conf Ser. 2022;2229(1):012020. [CrossRef].
15. Xia Y, Pan W, Wang J, Zhu C, Song M. Hybrid model based predictive control for temperature-humidity regulation in direct expansion air conditioning systems. J Build Eng. 2025;105:112560. [CrossRef].
16. Huang H, Luo Y, Zhao C, Suo H. Temperature control method for electric heating furnaces based on auto-encoder and fuzzy PI control. Sensors. 2025;25(16):5020. [CrossRef].
17. Cao F, Wang K, Xing Z, Shu P, Xue J. Experimental study on constant temperature and humidity air-conditioner with recovering condensing heat. J Xi'an Jiaotong Univ. 2008;42(5):524–50.
18. Schrock VE, Grossman LM. Forced convection boiling in tubes. Nucl Sci Eng. 1962;12(4):474–81. [CrossRef].
19. Youn B, Kim NH. An experimental investigation on the airside performance of fin-and-tube heat exchangers having sinusoidal wave fins. Heat Mass Transf. 2007;43(12):1249–62. [CrossRef].

20. Dittus FW, Boelter LMK. Heat transfer in automobile radiators of tubular type. Int Commun Heat Mass Transf. 1985;12:3–22. [CrossRef].
21. Shah MM. A general correlation for heat transfer during film condensation inside pipes. Int J Heat Mass Transf. 1979;22(4):547–56. [CrossRef].
22. Gu B, Peng WH, Zeng WJ. Research of air-side characteristics and correlations development for two different types of smooth wave fin-and-tube heat exchangers. J Refrig. 2020;41(3):25–30. [CrossRef].